NASA Technical Paper 1471

A Method for Obtaining Practical Flutter-Suppression Control Laws Using Results of Optimal Control Theory

Jerry R. Newsom

AUGUST 1979

NASA

NASA Technical Paper 1471

A Method for Obtaining Practical Flutter-Suppression Control Laws Using Results of Optimal Control Theory

Jerry R. Newsom
Langley Research Center
Hampton, Virginia

SUMMARY

A method is presented for using the results of optimal control theory to synthesize a feedback filter. The feedback filter is used to force the output of the filtered frequency response to match that of a desired optimal frequency response over a finite frequency range. This matching is accomplished by employing a nonlinear programing algorithm to search for the coefficients of the feedback filter that minimize the error between the optimal frequency response and the filtered frequency response. The method is applied to the synthesis of an active flutter-suppression control law for an aeroelastic wind-tunnel model. It is shown that the resulting control law suppresses flutter over a wide range of subsonic Mach numbers. The study indicates that this is a promising method for synthesizing practical control laws using the results of optimal control theory.

INTRODUCTION

In modern control theory, a number of methods have been developed to design control systems which require multiple variables (so-called state variables) to describe the state or condition of the system. Optimal regulator theory (ref. 1) is the most widely used method for determining optimal control laws that feed back all of the state variables (full-state feedback). Most applications of optimal regulator theory have been limited to problems with only a few state variables. Recently, however, this theory has been applied to aeroelastic problems that are generally characterized by a large number of state variables (ref. 2).

Several researchers have applied optimal regulator theory to active flutter suppression. The two-dimensional flutter problem was investigated by Lyons et al. (ref. 3) and Edwards (ref. 4). Their work was extended in reference 5 by considering a more complete mathematical model incorporating three-dimensional unsteady aerodynamics. It is shown in reference 5 that optimal regulator theory provides full-state feedback control laws that are very attractive for flutter suppression.

A major problem in the application of optimal regulator theory is the conversion of the theoretical (full-state feedback) control law into a practical control law (that is, one that can be readily implemented). This problem arises because optimal regulator theory normally requires that all state variables be available for feedback. Direct measurement of all feedback states for an aircraft wing, for example, is not possible, and a method is required to obtain a practical control law from the limited sensor measurements available. Konar et al. (ref. 6) developed such a method by adjusting the optimal full-state feedback gains to be compatible with sensor measurements. This method uses a numerical search algorithm in the time domain that adjusts feedback gains while maintaining the least amount of increase in the quadratic objective

function. This method has been applied to studies involving load alleviation for the C-5A (ref. 2).

The purpose of this paper is to describe a different approach that uses frequency domain techniques to obtain a practical control law. This approach employs a transfer-function matching technique developed by Coffey (ref. 7). This method uses a gradient optimization algorithm to design a feedback filter that forces the open-loop frequency response of the system to match a desired open-loop frequency response. In reference 7, it is assumed that the desired open-loop frequency response is known. The present approach defines the desired open-loop frequency response as that of the optimal full-state feedback system. Also given is a brief description of the method employed to develop the equations in terms of state variables. The technique is applied to the synthesis of a practical control law for active flutter suppression of an aero-elastic wind-tunnel model.

SYMBOLS

a_i ith denominator coefficient of actuator transfer function

b_o numerator coefficient of actuator transfer function

c reference length, m

c_c steamwise local chord, m

E error function in frequency domain

f frequency, Hz

$f(s)$ factor in feedback filter

g gravitational constant, 9.80 m/sec^2

$H(s)$ feedback-filter transfer function

i $= \sqrt{-1}$

J quadratic optimization cost function

K_f scalar gain for feedback filter

k reduced frequency, $\dfrac{c\omega}{2U}$

L number of frequencies

M number of aerodynamic lag terms

q_f flutter dynamic pressure, kPa

2

q_∞ free-stream dynamic pressure, $\frac{1}{2}\rho U_\infty^2$, kPa

s   Laplace variable

t   time, sec

U_∞ free-stream velocity, m/sec

u   control input

$\hat{u}$ practical control input

$\bar{u}$ optimal control input

w_g vertical gust velocity, m/sec

y   output variable

z   vertical displacement, m

β_m aerodynamic lag terms

δ control surface position, positive down, deg

δ_c actuator command, deg

ζ damping ratio

ω circular frequency, rad/sec

ω_n natural frequency, rad/sec

Matrices:

[A]   total-system dynamics matrix

$[A_a]$ actuator dynamics matrix

$[A_i]$ real aerodynamic matrix coefficients

$[A_v]$ vehicle dynamics matrix

[A(ik)]   generalized aerodynamic-force matrix due to wing motion

[B]   total-system control distribution matrix

$[B_a]$ actuator control distribution matrix

$[B_v]$ vehicle control distribution matrix

$[C]$	total-system state-coefficient output matrix
$[C_a]$	actuator state-coefficient output matrix
$[C_s]$	generalized damping matrix
$[C_v]$	vehicle state-coefficient output matrix
$\lfloor C_\phi \rfloor$	row matrix of mode-shape amplitudes
$[D_v]$	vehicle input-coefficient output matrix
$[D(ik)]$	generalized aerodynamic-force matrix due to control surface rotation
$\{G(ik)\}$	generalized aerodynamic-force vector due to vertical gust velocity
$[I]$	identity matrix
$[K]$	optimal gain matrix
$[K_s]$	generalized stiffness matrix
$[M_s]$	generalized mass matrix
$[P]$	Riccati matrix
$[Q]$	output weighting matrix
$\{q\}$	generalized coordinate vector
$[R]$	control weighting matrix
$\{u\}$	total-system input vector
$\{u_a\}$	actuator input vector
$\{u_v\}$	vehicle input vector
$\{\bar{u}\}$	optimal control input vector
$\{x\}$	total-system state vector
$\{x_a\}$	actuator state vector
$\{x_v\}$	vehicle state vector
$\{Y\}$	total-system output vector
$\{Y_a\}$	actuator output vector
$\{Y_v\}$	vehicle output vector

$\{\delta\}$ control surface position vector

Subscripts:

f   flutter

I   imaginary part of complex value

R   real part of complex value

rms   root-mean-square value

    Dots over symbols denote derivatives with respect to time.

EQUATIONS OF MOTION

    The equations of motion for a flexible vehicle may be expressed in matrix form as

$$[M_S]\{\ddot{q}\} + [C_S]\{\dot{q}\} + [K_S]\{q\} + q_\infty[A(ik)]\{q\} + q_\infty[D(ik)]\{\delta\} = q_\infty\{G(ik)\}\frac{w_g}{U} \qquad (1)$$

where

$[M_S]$ generalized mass matrix

$[C_S]$ generalized damping matrix

$[K_S]$ generalized stiffness matrix

$[A(ik)]$ generalized aerodynamic-force matrix due to wing motion

$[D(ik)]$ generalized aerodynamic-force matrix due to control surface rotation

$\{G(ik)\}$ generalized aerodynamic-force vector due to vertical gust velocity

    In flutter analyses where unsteady aerodynamics are of major importance, the aerodynamic-force matrices are normally represented as tabular functions of reduced frequency $k = c\omega/2U$. With the unsteady aerodynamic forces in this form, the equations of motion cannot be written as a set of first-order differential (state-space) equations. The equations can be cast into state-space form, however, by use of aerodynamic approximation functions (refs. 8 and 9).

Aerodynamic Approximation Functions and State-Space Equations

    The techniques for developing the aerodynamic approximation equations and the state-space equations are similar to those described in references 5 and 10. The aerodynamic approximation technique involves fitting the curve of a mathematical function of ik to the aerodynamic forces. Each element of the

5

aerodynamic-force matrix is fit with an approximation function of the form

$$[A(ik)] = [A_0] + [A_1] (ik) + [A_2] (ik)^2 + \sum_{m=1}^{M} \frac{[A_{m+2}] (ik)}{\beta_m + (ik)} \qquad (2)$$

The aerodynamic lag terms β_m are somewhat arbitrary but are usually chosen to lie somewhere within the range of interest of the reduced frequencies. The numerator matrices are computed to give a least-square error for the values of k at which the aerodynamic forces are known.

As described in reference 5, substituting equation (2) into equation (1) and equating derivatives to the powers of the Laplace operator $(s = i\omega = (2U/c)ik)$ yields the equations of motion for the basic vehicle. Written in standard state-space form,

$$\left. \begin{array}{l} \{\dot{X}_v\} = [A_v]\{X_v\} + [B_v]\{u_v\} \\[2mm] \{Y_v\} = [C_v]\{X_v\} + [D_v]\{u_v\} \end{array} \right\} \qquad (3)$$

The elements of the vehicle state vector $\{X_v\}$ are the generalized coordinates and their derivatives. The vehicle input vector $\{u_v\}$ consists of the control surface displacement, the gust disturbance, and their derivatives. The order of the derivatives depends on the number of lag terms used in the aerodynamic approximation.

Actuator Models

To include the effect of actuator dynamics during design of the optimal control law, the actuator model is described in state-space form and then interconnected to the basic vehicle equations. Actuator models are generally represented by transfer functions. Consider an actuator transfer function of the following form:

$$\frac{\delta(s)}{\delta_c(s)} = \frac{b_0}{s^n + a_{n-1}s^{n-1} + \ldots a_0} \qquad (4)$$

By cross multiplying and equating derivatives to the powers of s, an nth order differential equation of the actuator can be written

$$\frac{d\delta}{dt^n} + a_{n-1} \frac{d\delta}{dt^{n-1}} + \ldots a_0\delta = b_0\delta_c \qquad (5)$$

By making the substitutions that $X_i = d^{i-1}\delta/dt^{i-1}$, a set of n first-order differential equations can be written. Thus,

$$\{\dot{X}_a\} = [A_a]\{X_a\} + [B_a]\{u_a\} \qquad (6)$$

where

$$\{X_a\} = \begin{Bmatrix} \delta \\ \dot{\delta} \\ \cdot \\ \cdot \\ \cdot \\ d^{n-1}\delta/dt^{n-1} \end{Bmatrix} \quad [A_a] = \begin{bmatrix} 0 & 1 & 0 & 0 & \cdots \\ 0 & 0 & 1 & 0 & \cdots \\ \cdot & \cdot & \cdot & \cdot & \cdot \\ \cdot & \cdot & \cdot & \cdot & \cdot \\ \cdot & \cdot & \cdot & \cdot & \cdot \\ -a_0 & -a_1 & \cdots & \cdots & -a_n \end{bmatrix} \quad [B_a] = \begin{bmatrix} 0 \\ 0 \\ \cdot \\ \cdot \\ \cdot \\ b_0 \end{bmatrix}$$
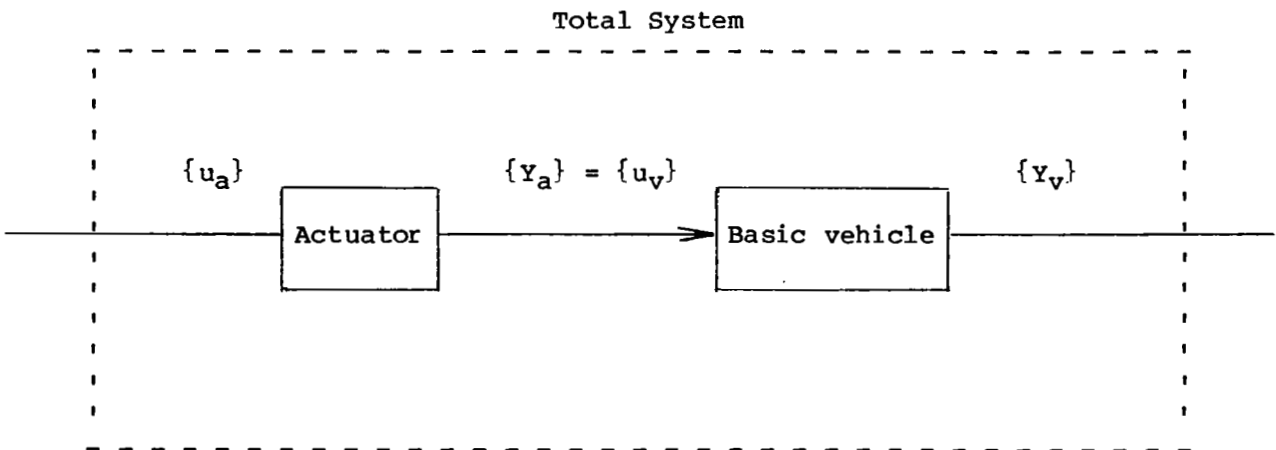
The output equations of the actuator are written in the form

$$\{Y_a\} = [C_a]\{X_a\} \tag{7}$$

where

$$[C_a] = \begin{bmatrix} 1 & 0 & 0 & \cdots \\ 0 & 1 & 0 & \cdots \\ \cdot & \cdot & \cdot & \cdot \\ \cdot & \cdot & \cdot & \cdot \\ \cdot & \cdots & \cdots & \cdots \end{bmatrix}$$

The interconnection of the actuator to the basic vehicle involves equating the output of the actuator to the input of the basic vehicle, as illustrated in the following sketch:

Total System

By using the relationship $\{u_v\} = \{Y_a\}$, the total-system equations can be written as

$$\left\{\begin{array}{c} \dot{X}_a \\ \dot{X}_v \end{array}\right\} = \left[\begin{array}{cc} A_a & 0 \\ B_v C_a & A_v \end{array}\right] \left\{\begin{array}{c} X_a \\ X_v \end{array}\right\} + \left[\begin{array}{c} B_a \\ 0 \end{array}\right]\{u_a\}$$

$$\{Y_v\} = [D_v C_a \quad C_v]\left\{\begin{array}{c} X_a \\ X_v \end{array}\right\}$$

(8)

or

$$\{\dot{x}\} = [A]\{x\} + [B]\{u\}$$

$$\{Y\} = [C]\{x\}$$

(9)

SYNTHESIS OF AN ACTIVE FLUTTER-SUPPRESSION CONTROL LAW

Regulator Theory

Optimal regulator theory provides for the minimization of a quadratic cost function of the output and control vectors (ref. 1). To find the optimal full-state feedback control law, the quadratic cost function

$$J = \int_0^\infty \left(\{Y\}^T [Q]\{Y\} + \{u\}^T [R]\{u\}\right) dt$$

(10)

is minimized. This leads to the optimal control law

$$\{u\} = \{\bar{u}\} = [K]\{x\}$$

$$[K] = -[R]^{-1} [B]^T [P]$$

(11)

For the time invariant (constant-coefficient differential equations) condition, [P] is the steady state solution of the matrix Riccati equation.

$$[P][A] + [A]^T [P] - [P][B][R]^{-1} [B]^T [P] + [Q] = 0$$

(12)

The application of regulator theory is an iterative process of selecting the appropriate cost function through changes in the weighting matrices [Q] and [R]. The procedure can be summarized as follows:

8

Step 1: Define the output ({Y}) and input ({u}) vectors that relate to the performance goals. (For example, minimum control surface displacement.)

Step 2: Select initial weighting matrices [Q] and [R]. (For example, see refs. 1 to 5.)

Step 3: Solve equations (11) and (12) for the optimal gains ([K]), thus minimizing the quadratic cost function J.

Step 4: Evaluate the design, and adjust weighting matrices until performance goals are met.

The optimal control law requires the capability to feed back all of the state variables. Since the description of the system involves modal or generalized coordinates in addition to physical coordinates, direct measurement of all state variables is not feasible. Only a linear combination of the state variables can be measured. Therefore, a method is employed which uses the available measurements.

Process for Design of Practical Control Law

The process described herein for the design of a practical control law is performed in the frequency domain and attempts to match a desired open-loop frequency response. The desired open-loop frequency response is that of the optimal full-state feedback system. The design process involves finding the coefficients of a feedback filter $H(s)$ that minimize the deviation of the open-loop frequency response $(\hat{u}/u)(i\omega)$ from the optimal open-loop frequency response $(\bar{u}/u)(i\omega)$. (See fig. 1.) Figure 2 is a Nyquist diagram illustrating the results of the design process for a practical control law. The objective is to make the deviation from the optimal system small. If this objective is met, the performance of the practical system will be similar to that of the optimal system.

Error function.- The error function is defined as the difference of $(\hat{u}/u)(i\omega)$ and $(\bar{u}/u)(i\omega)$ over a set of frequency points ω_i $(i = 1, 2, . . ., L)$, for which a close fit is desired. The closeness of $(\hat{u}/u)(i\omega)$ to $(\bar{u}/u)(i\omega)$ can be described mathematically by

$$E = \left[\frac{\bar{u}}{u}(i\omega)^* - \frac{\hat{u}}{u}(i\omega)^*\right]^T\left[\frac{\bar{u}}{u}(i\omega) - \frac{\hat{u}}{u}(i\omega)\right] \tag{13}$$

where the asterisk (*) denotes the complex conjugate, with

$$\left.\begin{aligned}
\frac{\bar{u}}{u}(i\omega) &= \left[\frac{\bar{u}}{u}(i\omega_1),\ \frac{\bar{u}}{u}(i\omega_2),\ \ldots,\ \frac{\bar{u}}{u}(i\omega_L)\right] \\[2em]
\frac{\hat{u}}{u}(i\omega) &= \left[\frac{\hat{u}}{u}(i\omega_1),\ \frac{\hat{u}}{u}(i\omega_2),\ \ldots,\ \frac{\hat{u}}{u}(i\omega_L)\right]
\end{aligned}\right\} \tag{14}$$

Feedback-filter design variables.- The form of the feedback filter $H(s)$ to be used is

$$H(s) = K_f\ \frac{\displaystyle\prod_{i=1}^{m}(s^2 + 2\zeta_i\omega_{ni}s + \omega_{ni}^2)}{\displaystyle\prod_{j=1}^{n}(s^2 + 2\zeta_j\omega_{nj}s + \omega_{nj}^2)}\ f(s) \tag{15}$$

The design variables are the gain K_f, the damping ratios ζ, and the frequencies ω_n (of each second-order factor in eq. (15)). The function $f(s)$ is included to help achieve any desired characteristics of the feedback filter, such as high-frequency roll-off. The procedure can be described as follows:

Step 1: Compute the optimal frequency response $\bar{u}/u$.

Step 2: Compute the frequency response between the output y and the control u.

Step 3: Choose the initial number of numerator factors m and denominator factors n of the filter.

Step 4: Choose a $f(s)$ to incorporate any desired characteristics of the filter, such as high-frequency roll-off.

Step 5: Minimize the error function E by using an optimization algorithm such as that of Davidon (ref. 11) and Fletcher and Powell (ref. 12).

Step 6: Examine the practical open-loop frequency response (Nyquist diagram) to establish any possible changes to $f(s)$.

Step 7: If any changes to $f(s)$ are established, repeat step 5.

Step 8: Repeat steps 3 through 7 for a family of m and n.

Step 9: Select the values of m, n, and f(s) that provide the smallest value of E.

APPLICATION OF TECHNIQUE

The methodology described previously is applied to the synthesis of an active flutter-suppression control law for an aeroelastic wind-tunnel model. The model geometry is shown in figure 3. The model consists of a cantilever wing with a 20-percent-chord, trailing-edge control surface located between the 76-percent and 89-percent semispan stations. The flutter-suppression sensor (accelerometer) is located at the 60-percent-chord and 92-percent-semispan station. The first eight elastic modes[1] are used as generalized coordinates covering a frequency range from 5.23 Hz to 118.15 Hz. The calculations necessary to determine the coefficients of the equations of motion (eq. (1)) are described in detail in reference 10.

Basic Wing Characteristics

Each of the aerodynamic terms is approximated in the s-plane through the use of equation (2) with M = 2. The β_m terms are varied until an acceptable curve fit is found. This resulted in the β_m terms being selected as 0.225 and 0.500 for all aerodynamic terms. In figure 4, one of the calculated oscillatory aerodynamic terms is compared with the approximation function at Mach = 0.9. In general, all of the aerodynamic terms have a good curve fit.

To validate the mathematical model further, the flutter boundary of the model without the flutter-suppression system (FSS off) is calculated. For a specific Mach number, the characteristic roots of equation (3) are found for a series of dynamic pressures. The dynamic pressure at which the real part of one of the roots becomes zero is the flutter dynamic pressure. Shown in figure 5 are the dynamic-pressure root loci at Mach = 0.9. Calculations of the dynamic-pressure root loci were also performed at Mach = 0.6, 0.7, and 0.8 to establish the FSS-off flutter boundary shown in figure 6. A comparison of the experimental results reported in reference 10 with these analyses indicates good agreement.

In addition to verifying the aerodynamic approximations with respect to the basic flutter characteristics, the transfer function between acceleration and control surface deflection (FSS off) is compared to that using the original, oscillatory aerodynamic forces. In this manner, the approximations for the control surface aerodynamic terms are verified. The gain and phase curves for this transfer function using the original oscillatory aerodynamics (designated as k-plane) and using the aerodynamic approximation function (designated as s-plane) are shown in figure 7 for comparison. Good agreement is indicated in both gain and phase.

---

[1]The two inplane modes (3 and 8) of reference 10 are omitted in this study.

The design condition for the FSS is chosen to be a 44-percent increase in flutter dynamic pressure at Mach = 0.9. The FSS is required to increase the flutter dynamic pressure by at least 44 percent at each of four Mach numbers (0.6, 0.7, 0.8, and 0.9) and, at the 44-percent margins, to exhibit ±6 dB gain margins and ±30° phase margins. In addition, the control surface activity can not exceed 6° (rms) and 600°/sec (rms). The optimal control laws are determined by solving equations (11) and (12) and thus satisfying equation (10). Equation (12) is solved using the computational algorithm developed by Vaughan (ref. 13) as coded in reference 14. For the quadratic optimization, zero-state weighting ([Q] = 0) is selected since this yields a set of gains that are "cheapest" (ref. 15) in terms of control input amplitude. This optimal full-state feedback control law leaves all stable eigenvalues unchanged and relocates the unstable eigenvalues to their mirror image in the left half plane. Once the full-state feedback gain matrix is determined, the optimal Nyquist diagram for the single input system is constructed by solving

$$\frac{\bar{u}(i\omega)}{u(i\omega)} = \lfloor K \rfloor [i\omega I - A]^{-1} \{B\} \tag{16}$$

Equation (16) is solved for a series of frequencies from 1 rad/sec to 301 rad/sec at increments of 3 rad/sec. The resulting Nyquist diagram (fig. 8) is a counterclockwise circle of radius unity centered on the (-1, 0) point. The full-state feedback control law provides gain and phase margins of -6 dB and ±60°, respectively. Note that the Nyquist diagram crosses the real axis only once (-6 dB) and, therefore, has infinite positive gain margin.

To synthesize a practical control law from the full-state feedback control law, the frequency response between sensor output and control surface input is established first. Using the accelerometer location shown in figure 3, the output frequency response is calculated by

$$\frac{\ddot{z}(i\omega)}{u(i\omega)} = \lfloor C_\phi \rfloor [i\omega I - A]^{-1} \{B\} \tag{17}$$

where $\lfloor C_\phi \rfloor$ is a row matrix of mode-shape amplitudes at the sensor location. The problem is to find the coefficients of the feedback filter $H(i\omega)$ that satisfy

$$\frac{\ddot{z}(i\omega)}{u(i\omega)} \times H(i\omega) \cong \frac{\bar{u}(i\omega)}{u(i\omega)} \tag{18}$$

over a finite set of frequency points ω_i (i = 1, . . ., L). In the frequency plane, equation (15) has the form

$$H(i\omega) = K_f \frac{\prod\limits_{i=1}^{m} \left[(i\omega)^2 + 2\zeta_i\omega_{ni}(i\omega) + \omega_{ni}^2 \right]}{\prod\limits_{j=1}^{n} \left[(i\omega)^2 + 2\zeta_j\omega_{nj}(i\omega) + \omega_{nj}^2 \right]} f(i\omega) \tag{19}$$

Employing a trial and error approach, various values of m and n are tried, and the combination that provides the smallest value of E ($m = 2$, $n = 2$) is determined. The low-frequency (3 rad/sec to 60 rad/sec) portion of the open-loop frequency response (not shown) indicated the need for an integrator. Therefore the $f(i\omega)$ is selected to be $1/(i\omega)$. The error function is again minimized with the previously determined values of m and n and the $1/(i\omega)$ in the filter. Figure 9 is the Nyquist diagram resulting from the minimization process. Since the optimization algorithm did not result in a -6 dB gain margin, the gain K_f was increased until a gain margin of -6 dB was achieved which resulted in the following control law:

$$\frac{\delta}{\ddot{z}} = \frac{2214}{s} \frac{s^2 + 2(0.127)(121.21)s + (121.21)^2}{s^2 + 2(0.962)(297.62)s + (297.62)^2}$$

$$\times \frac{s^2 + 2(0.088)(269.14)s + (269.14)^2}{s^2 + 2(0.964)(294.91)s + (294.91)^2} \left(\frac{\text{deg}}{\text{g}}\right) \tag{20}$$

Figure 10 is a Nyquist diagram obtained by using the control law defined by equation (20).

Results

The performance of the control law in terms of increased flutter dynamic pressure, root-mean-square (rms) values of the control activity in turbulence, and gain/phase margins are examined at Mach = 0.6, 0.7, 0.8, and 0.9. All calculations are performed using a modified version of the computer program described in reference 16. A summary of these results is presented in table 1.

Flutter characteristics.- Dynamic-pressure root locus calculations are performed to establish the FSS-on flutter boundary. Shown in figure 11 are the FSS-on root loci at Mach = 0.9. The control law increases the damping of the flutter mode while having very little effect on the other modes. The increased damping delays flutter onset until $q_\infty = 9.863$ kPa, which is a 96-percent increase in flutter dynamic pressure. Large increases in flutter dynamic pressure are predicted at the other Mach numbers as illustrated by the FSS-on flutter boundary presented in figure 12.

Control surface activity.- Control surface activity in turbulence is determined using power-spectral-density (PSD) analyses similar to that described in reference 10. A Von Karman gust spectrum with a characteristic length of 30.48 m is used to simulate turbulence distribution and intensity in

13

the wind tunnel. The variations of δ_{rms} and $\dot{\delta}_{rms}$ with dynamic pressure at Mach = 0.6, 0.7, 0.8, and 0.9 are shown in figure 13. The largest values of δ_{rms} (5.5°) and $\dot{\delta}_{rms}$ (270°/sec) occur at the maximum dynamic pressure investigated (q_∞ = 10.773 kPa at Mach = 0.6). As indicated, δ_{rms} and $\dot{\delta}_{rms}$ are only slightly dependent on Mach number but highly dependent on dynamic pressure.

Gain and phase margins.- Nyquist diagrams are constructed at all four Mach numbers to establish gain and phase margins. The gain margins at the Mach 0.9 design condition are -6.27 and +13.60 dB with phase margins of -58.8° and 41.0°. (See fig. 10.) The Nyquist diagrams at the other Mach numbers (not shown) are similar in character to that at Mach 0.9. The gain and phase margins at all four Mach numbers are presented in table 1 for a dynamic pressure 44 percent above the FSS-off flutter boundary. Gain margins of approximately ±6 dB are exhibited at all four Mach numbers; however, the positive phase margins at the lower Mach numbers are less than the +30° requirement.

CONCLUDING REMARKS

A method is presented for synthesizing feedback control laws using optimal regulator theory. The method is applied to the synthesis of an active flutter-suppression control law for an aeroelastic wind-tunnel model. Important results of the study are:

1. It is shown that a practical flutter-suppression control law can be synthesized by use of a gradient optimization algorithm to design a feedback filter which minimizes the difference between the filtered frequency response and the optimal frequency response.

2. Application of the method to a wind-tunnel model provides a control law which is shown by analysis to be capable of increasing flutter dynamic pressure by at least 44 percent over a range of Mach numbers from 0.6 to 0.9.

Langley Research Center
National Aeronautics and Space Administration
Hampton, VA 23665
June 4, 1979

REFERENCES

1. Athans, Michael: The Role and Use of the Stochastic Linear-Quadratic-Gaussian Problem in Control System Design. IEEE Trans. Autom. Control, vol. AC-16, no. 6, Dec. 1971, pp. 529-552.

2. VanDierendonck, Albert J.; Stone, Charles R.; and Ward, Michael D.: Application of Practical Optimal Control Theory to the C-5A Load Improvement Control System (LICS). AFFDL-TR-73-122, U.S. Air Force, Oct. 1973. (Available from DDC as AD-776 297.)

3. Lyons, M. G.; Vepa, R.; McIntosh, S. C., Jr.; and DeBra, D. B.: Control Law Synthesis and Sensor Design for Active Flutter Suppression. AIAA Paper No. 73-832, Aug. 1973.

4. Edwards, John William: Unsteady Aerodynamic Modeling and Active Aero-elastic Control. SUDAAR 504 (NASA Grant NGL-05-020-007), Stanford Univ., Feb. 1977. (Available as NASA CR-148019.)

5. Newsom, Jerry Russell: Active Flutter Suppression Synthesis Using Optimal Control Theory. M.S. Thesis, The George Washington Univ., 1978.

6. Konar, A. F.; Stone, C. R.; Mahesh, J. K.; and Hank, M.: Active Control Synthesis for Flexible Vehicles. Volume 1 - KONPACT Theoretical Description. AFFDL-TR-75-146, U.S. Air Force, June 1976. (Available from DDC as AD-B015198L.)

7. Coffey, T. C.: Automatic Frequency-Domain Synthesis of Multiloop Control Systems. AIAA J., vol. 8, no. 10, Oct. 1970, pp. 1791-1798.

8. Roger, Kenneth L.: Airplane Math Modeling Methods for Active Control Design. Structural Aspects of Active Controls, AGARD-CP-228, Aug. 1977, pp. 4-1 - 4-11.

9. Vepa, Ranjan: On the Use of Pade Approximants To Represent Unsteady Aerodynamic Loads for Arbitrarily Small Motions of Wings. AIAA Paper No. 76-17, Jan. 1976.

10. Abel, Irving: An Analytical Technique for Predicting the Characteristics of a Flexible Wing Equipped With an Active Flutter-Suppression System and Comparison With Wind-Tunnel Data. NASA TP-1367, 1979.

11. Davidon, William C.: Variable Metric Method for Minimization. ANL-5990 Rev. (Contract W-31-109-eng-38), U.S. At. Energy Comm., Nov. 1959.

12. Fletcher, R.; and Powell, M. J. D.: A Rapidly Convergent Descent Method for Minimization. Computer J., vol. 6, no. 2, July 1963, pp. 163-168.

13. Vaughan, David R.: A Negative Exponential Solution for the Matrix Riccati Equation. IEEE Trans. Autom. Control, vol. AC-14, no. 1, Feb. 1969, pp. 72-75.

14. Armstrong, Ernest S.: ORACLS – A System for Linear-Quadratic-Gaussian Control Law Design. NASA TP-1106, 1978.

15. Kwakernaak, Huibert; and Sivan, Raphael: Linear Optimal Control Systems. John Wiley & Sons, Inc., c.1972.

16. Peele, Ellwood L.; and Adams, William M., Jr.: A Digital Program for Calculating the Interaction Between Flexible Structures, Unsteady Aerodynamics and Active Controls. NASA TM-80040, 1979.
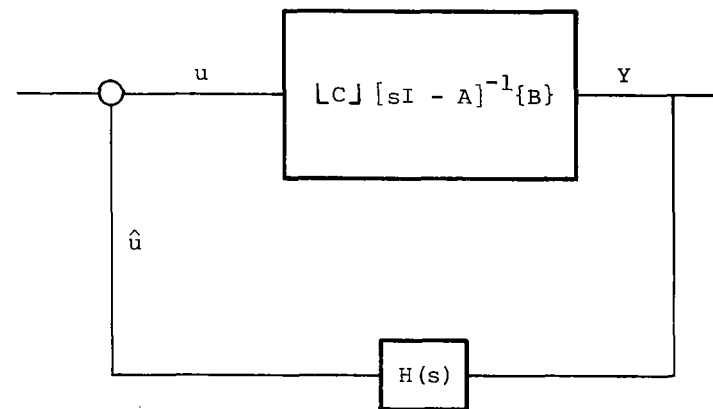
TABLE 1.- CONTROL LAW PERFORMANCE

Mach number	q_f (FSS off), kPa	q_f (FSS on), kPa (percent increase)	$1.44q_\infty$, kPa	δ_{rms}, deg	$\dot{\delta}_{rms}$, deg/sec	Gain margin, dB	Phase margin, deg
0.60	7.305	12.832 (75)	10.773	5.5	270	−5.89 +9.90	−33.0 +16.8
0.70	6.655	11.730 (78)	9.815	5.1	258	−6.24 +10.75	−32.4 +20.2
0.80	5.906	10.294 (76)	8.618	4.5	238	−6.49 +12.00	−41.0 +26.6
0.90	5.027	9.863 (96)	*7.661	4.0	209	−6.27 +13.60	−58.8 +41.2

*Design point.
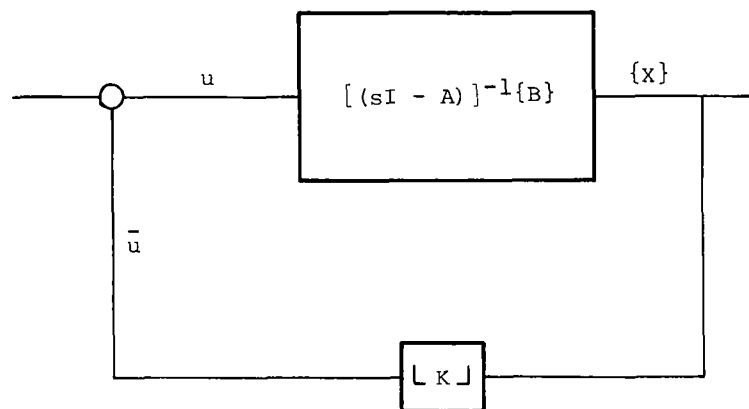
(a) Optimal.

(b) Practical.

Figure 1.- Block diagrams of optimal and practical control laws.
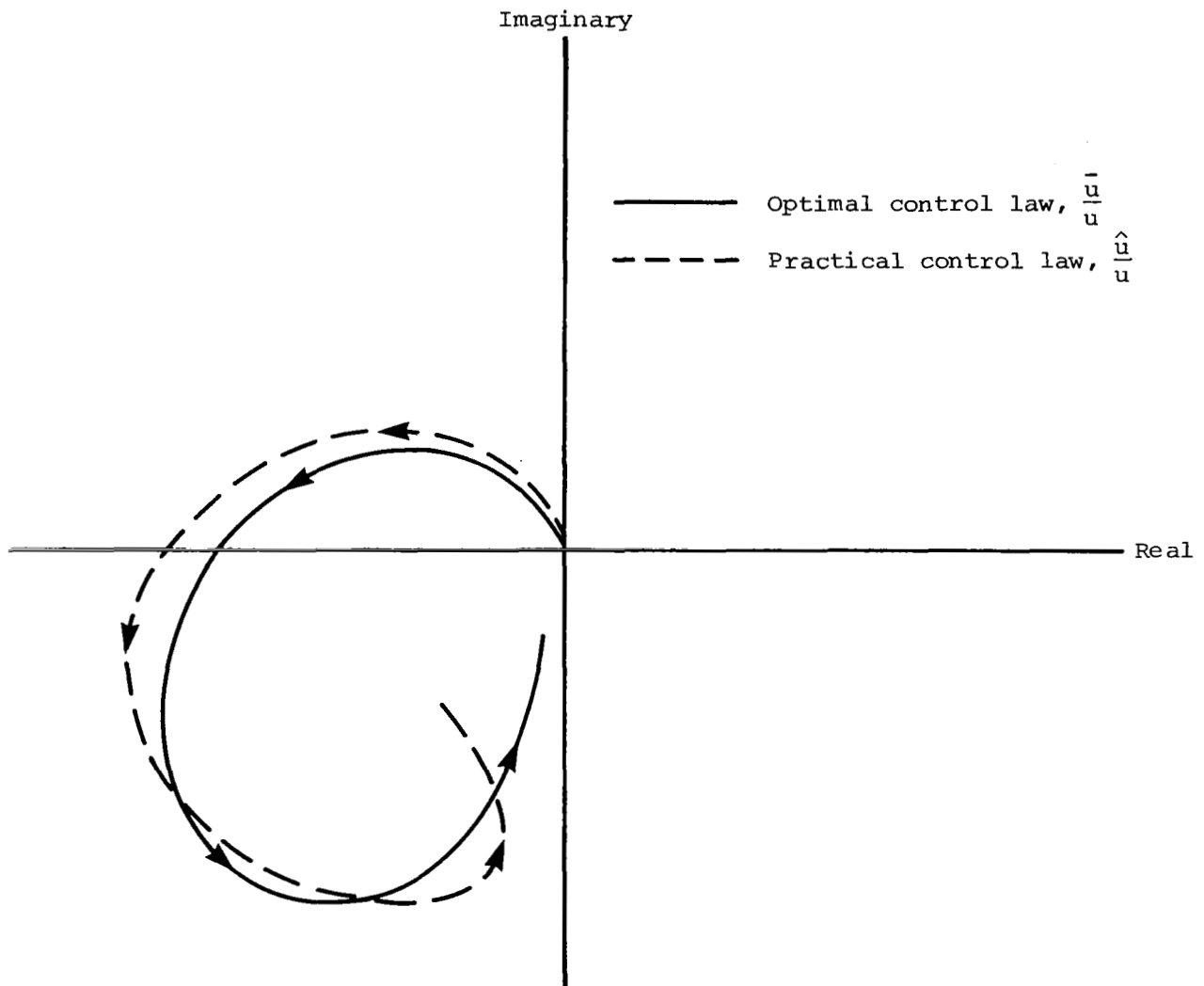
Figure 2.- Nyquist diagram illustrating control-law design method.
(Arrows indicate increasing frequency.)
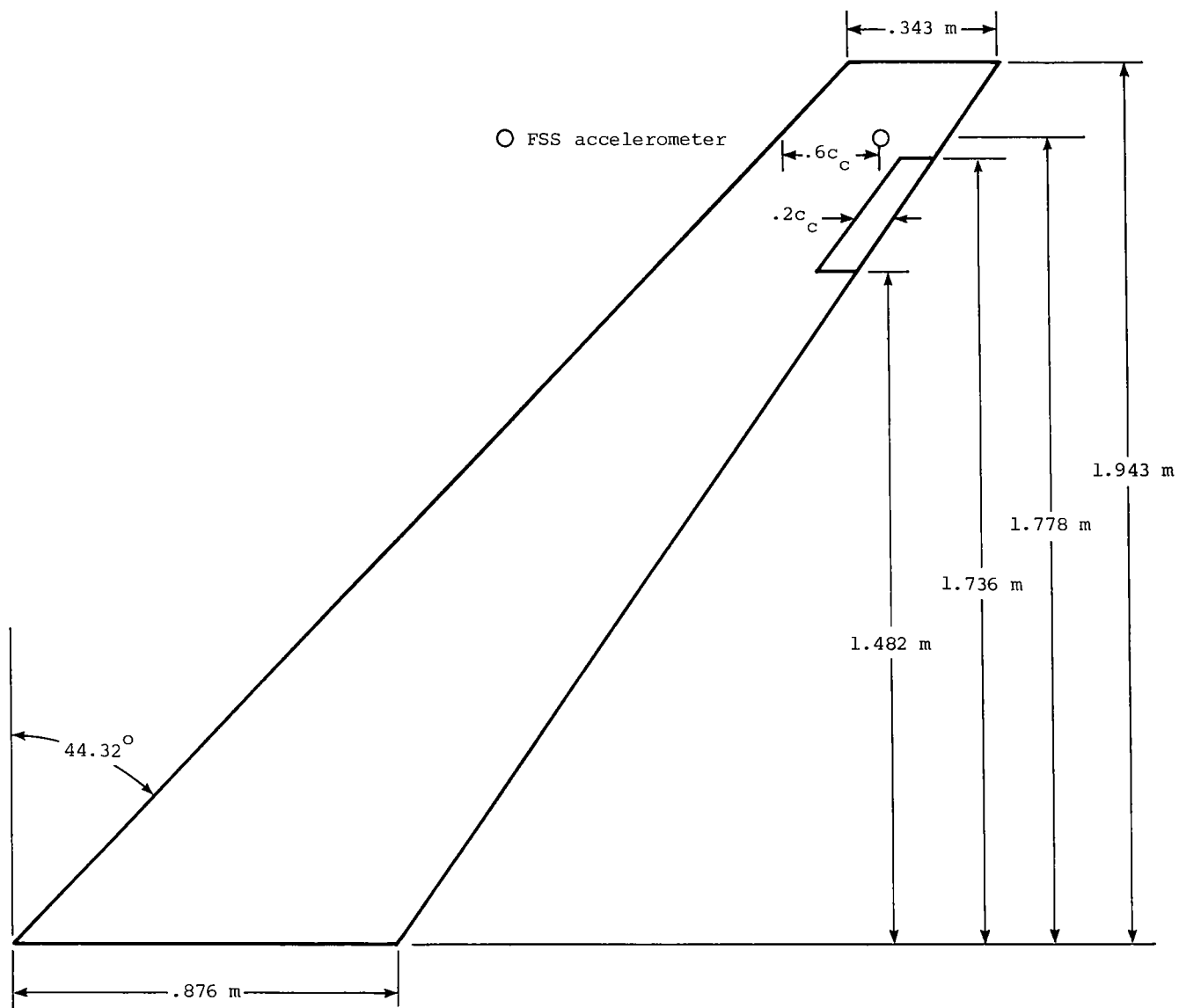
Figure 3.- Model geometry.
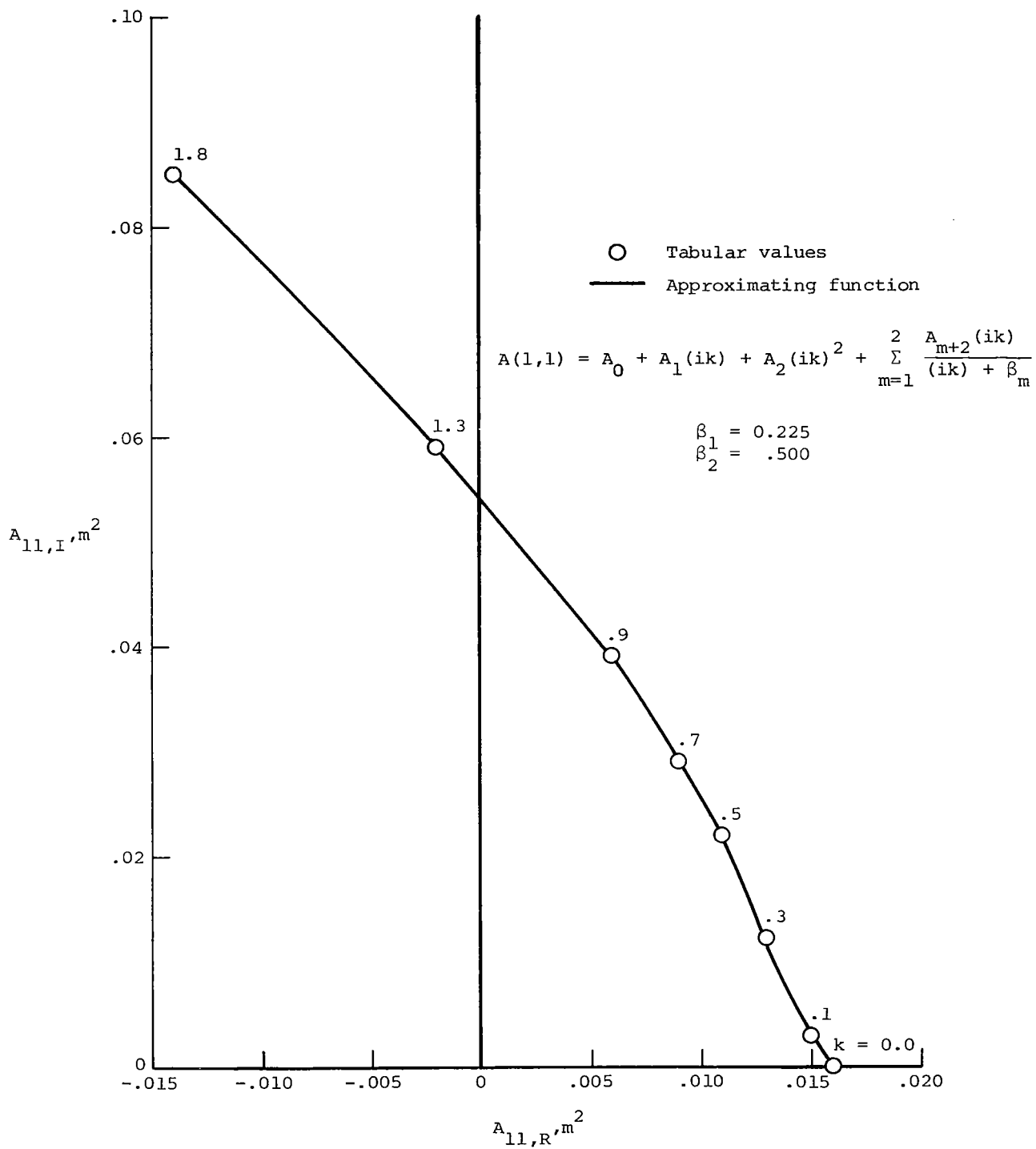
Figure 4.- Curve fit for A_{11} generalized aerodynamic force; Mach = 0.9.

$$A(1,1) = A_0 + A_1(ik) + A_2(ik)^2 + \sum_{m=1}^{2} \frac{A_{m+2}(ik)}{(ik) + \beta_m}$$
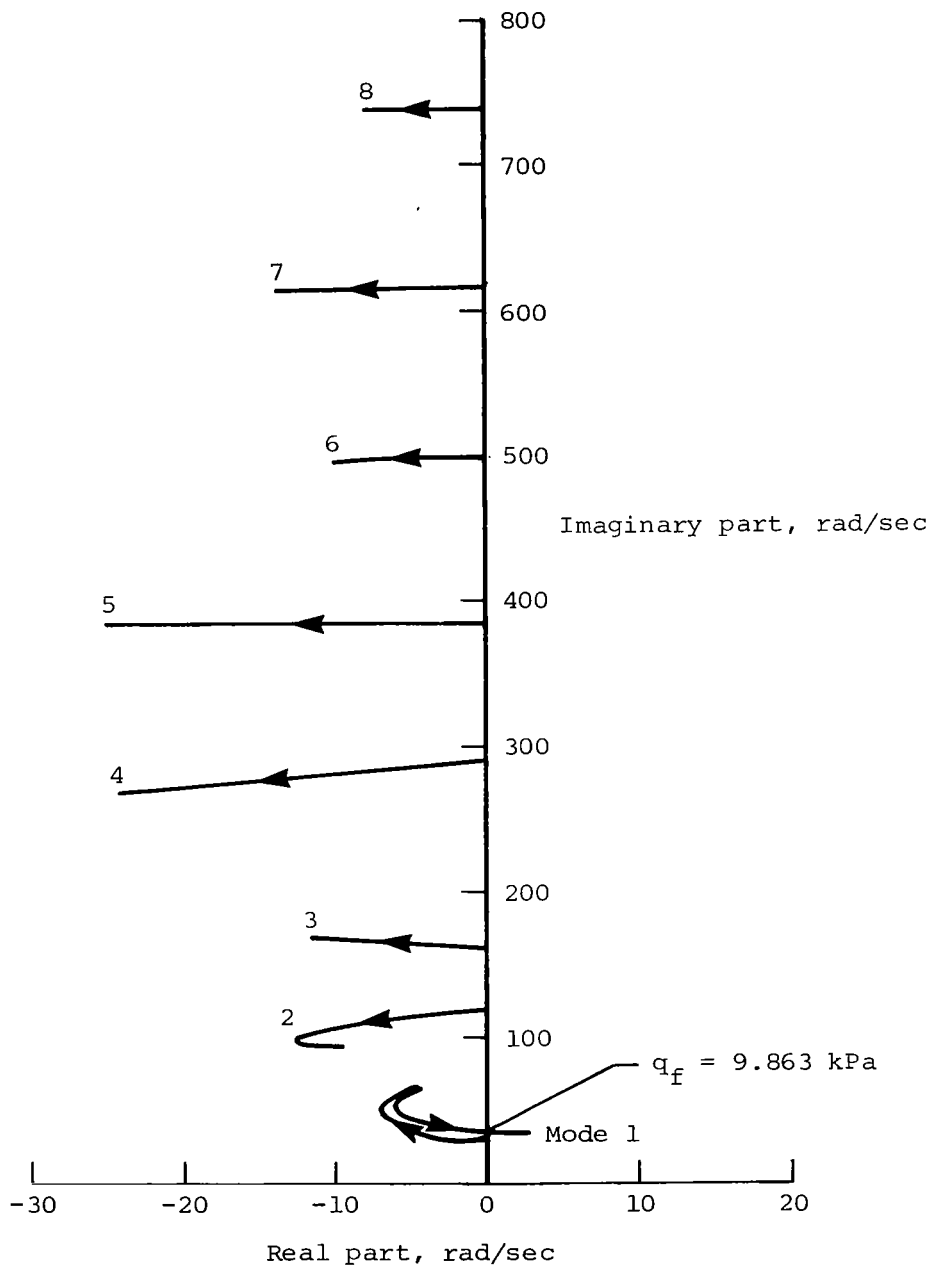
$\beta_1 = 0.225$
$\beta_2 = .500$
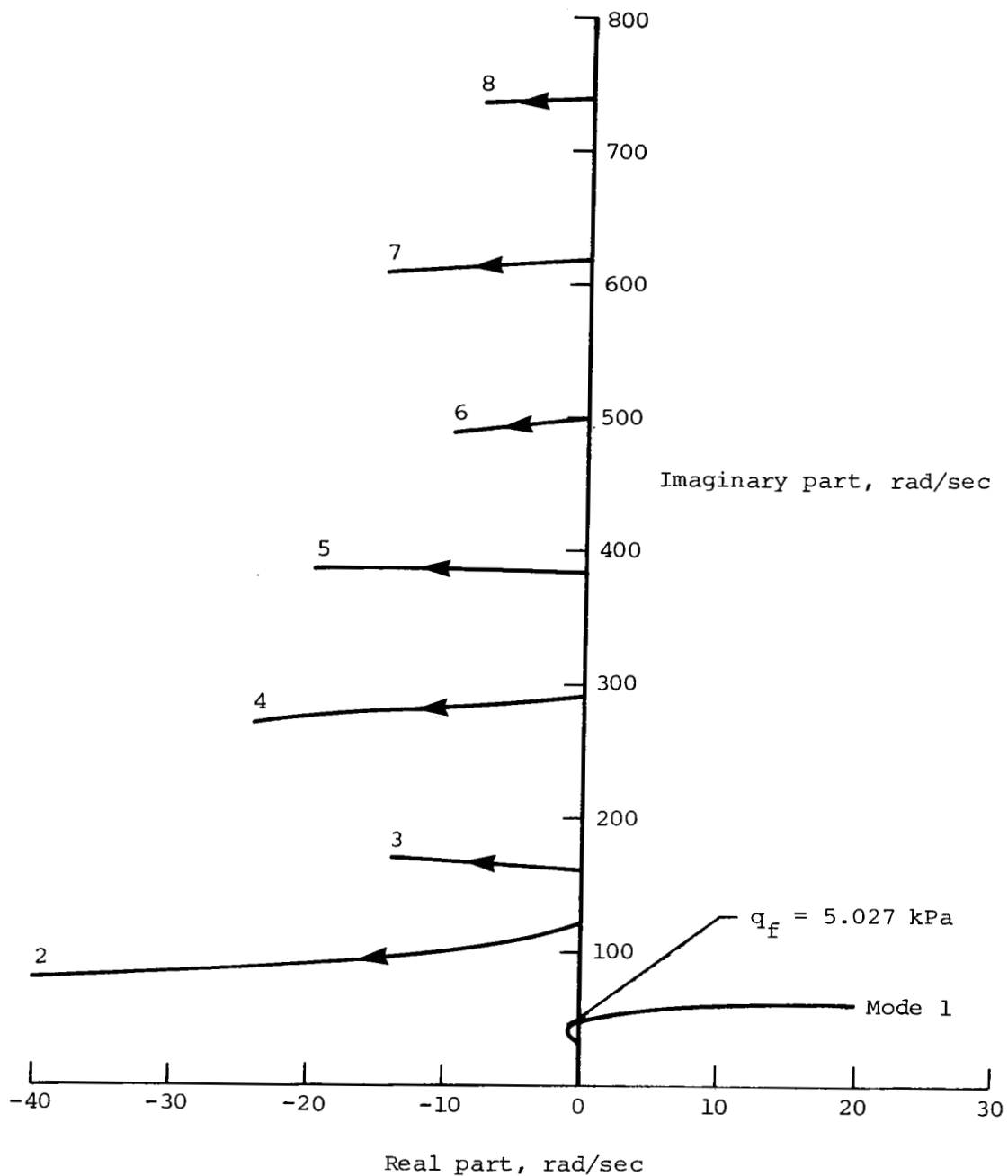
Figure 5.- Dynamic-pressure root loci; FSS off, Mach = 0.9.
(Arrows indicate increasing dynamic pressure.)
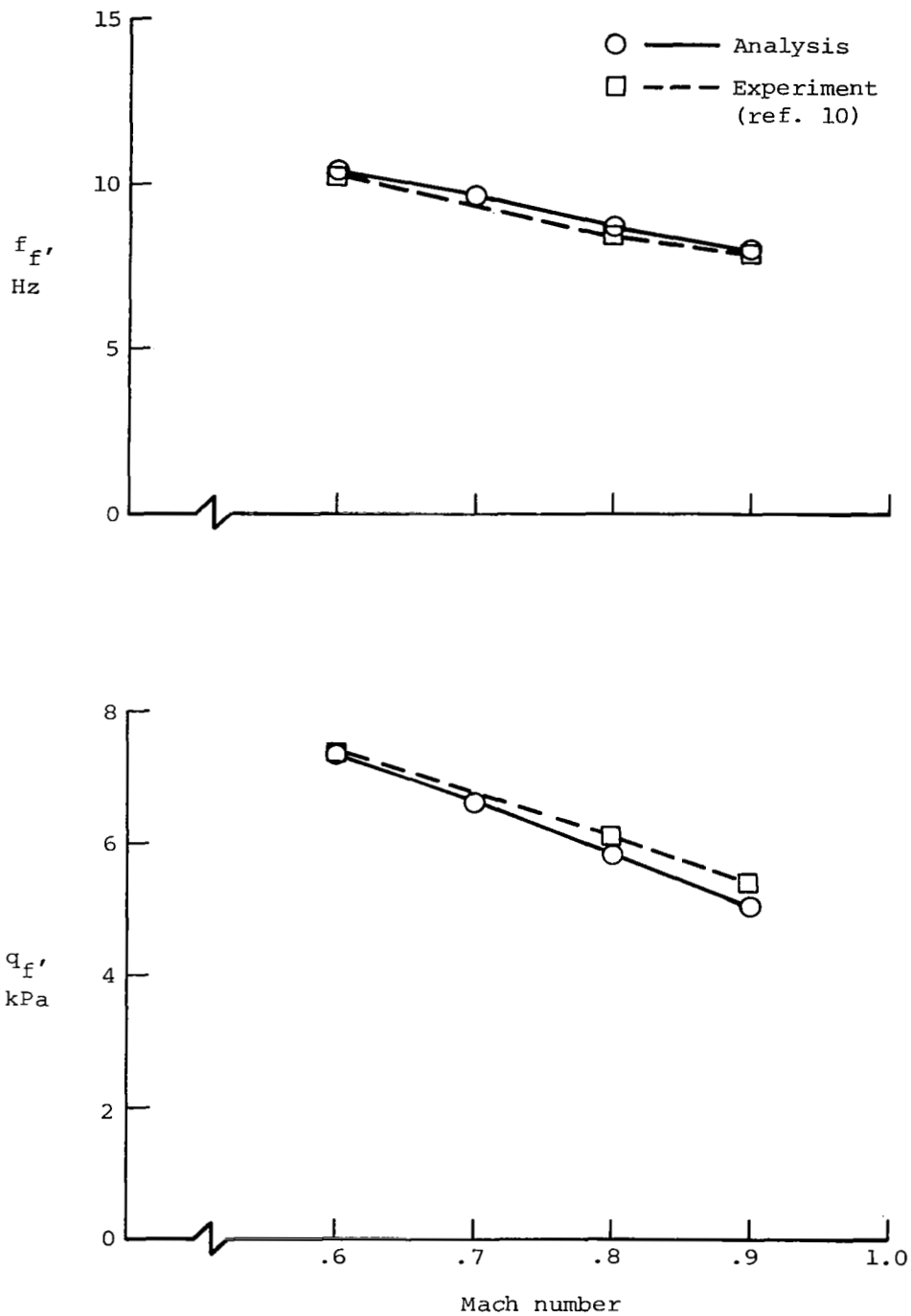
Figure 6.- Flutter boundary; FSS off.

(a) Gain.
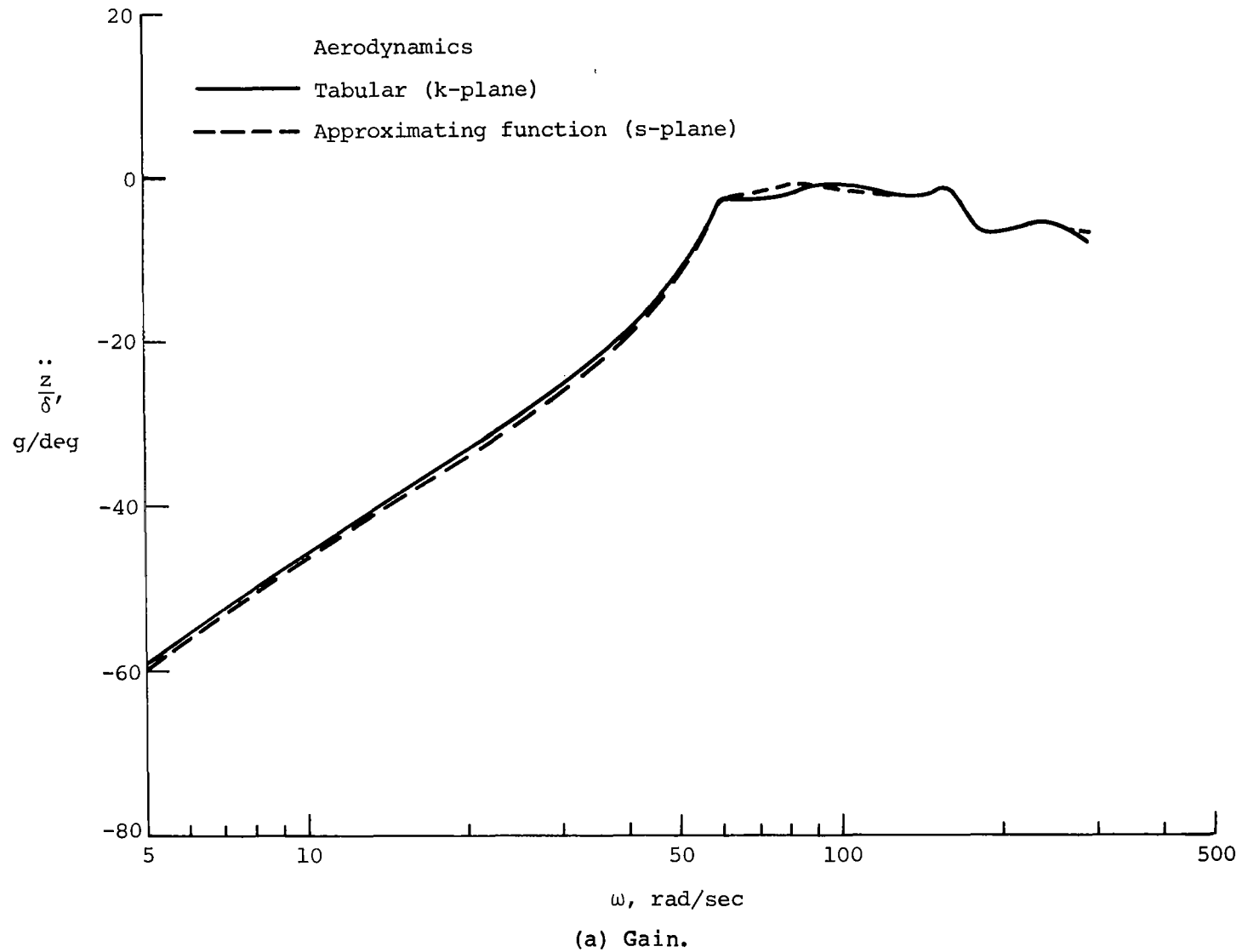
Figure 7.- Bode diagram of transfer function between acceleration and control surface input (FSS off); $q_\infty = 7.661$ kPa, Mach = 0.9. (Vertical axis is in decibels.)
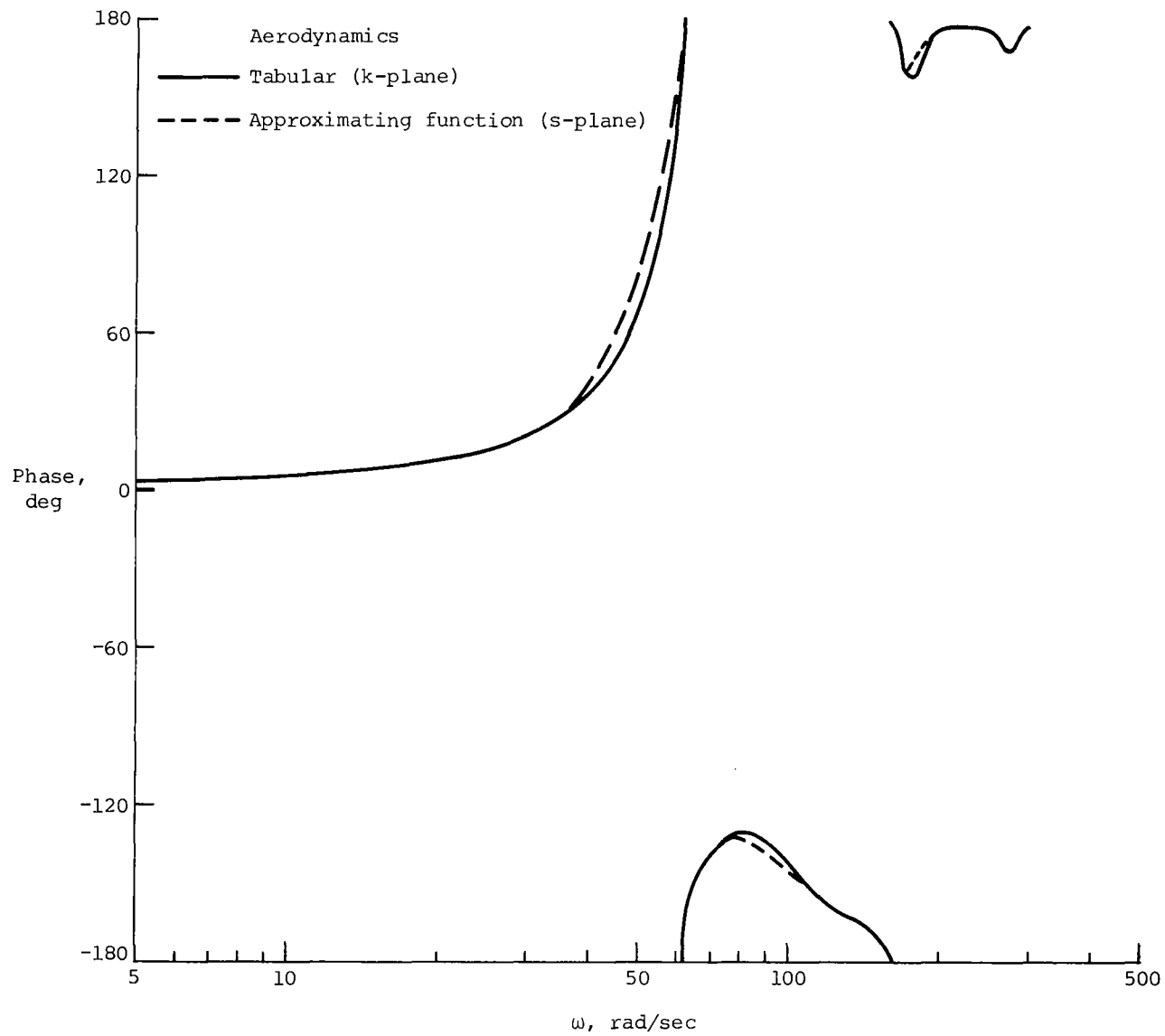
(b) Phase.

Figure 7.- Concluded.
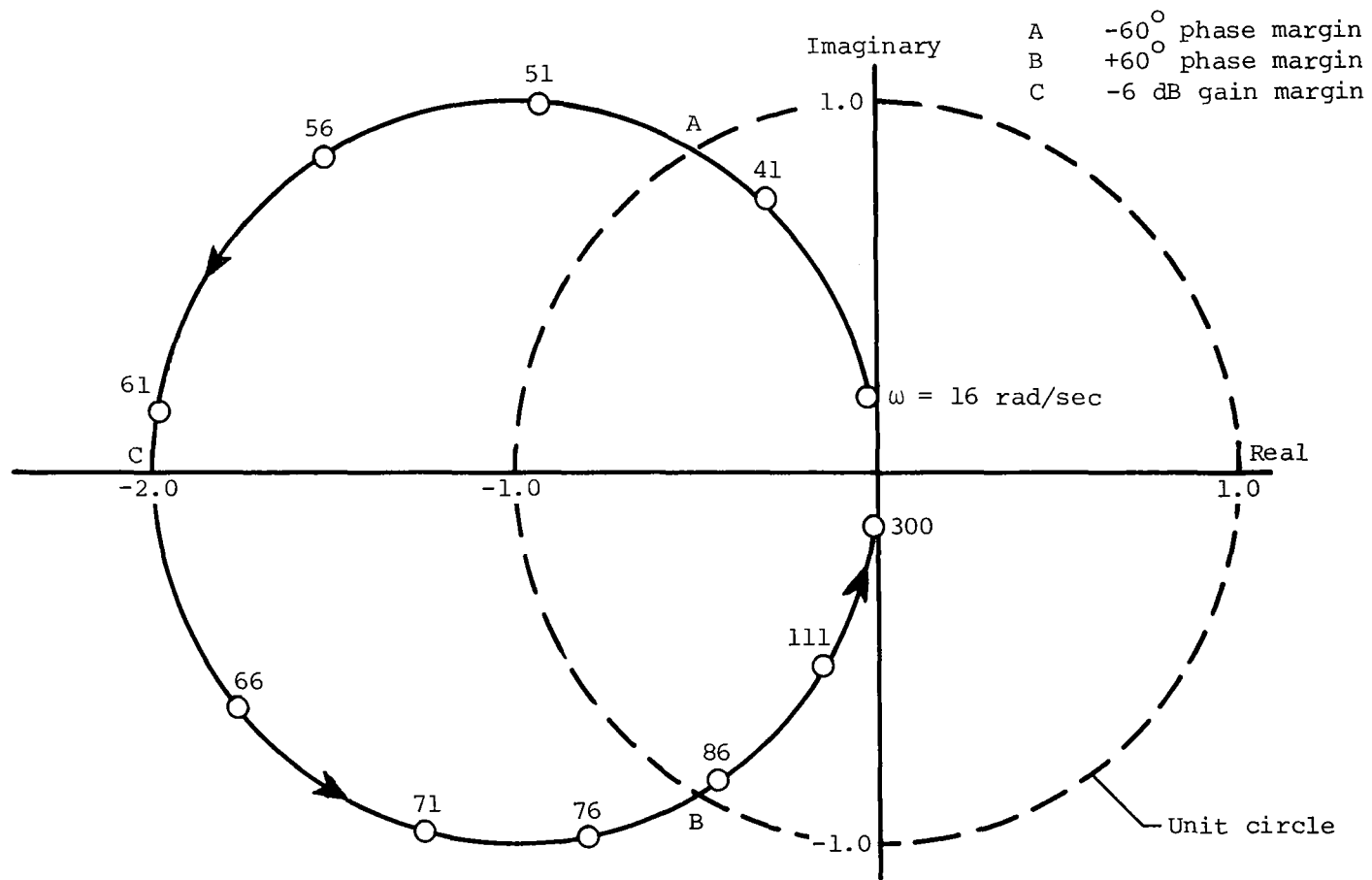
Figure 8.- Nyquist diagram of optimal control law; q_∞ = 7.661 kPa, Mach = 0.9.
(Arrows indicate increasing frequency.)
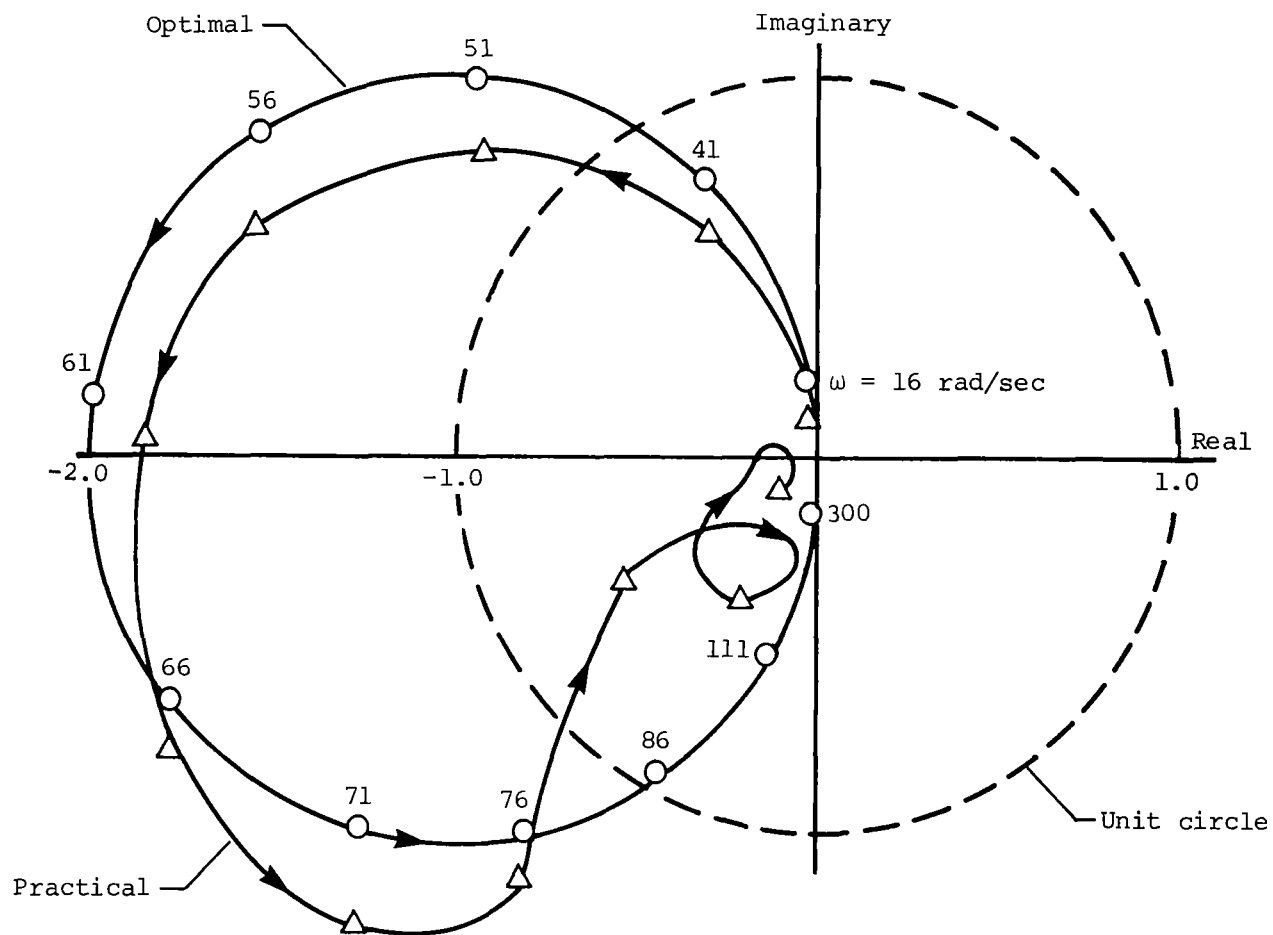
Figure 9.- Nyquist diagram of practical control law and optimal control law; q_∞ = 7.661 kPa, Mach = 0.9. (Arrows indicate increasing frequency.)
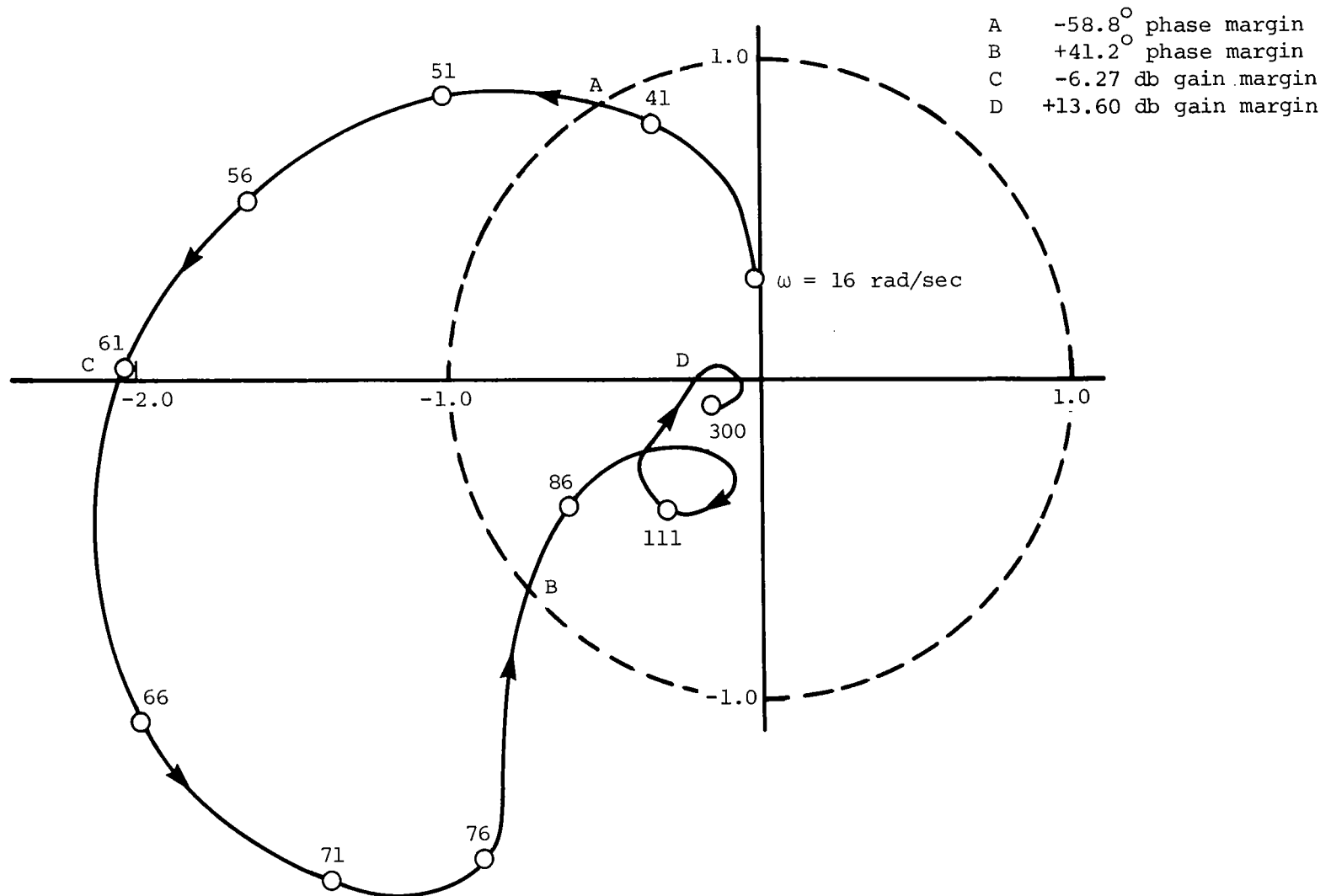
Figure 10.- Nyquist diagram of practical control law that meets design requirements; q_∞ = 7.661 kPa, Mach = 0.9. (Arrows indicate increasing frequency.)

Figure 11.- Dynamic-pressure root loci; FSS on, Mach = 0.9.
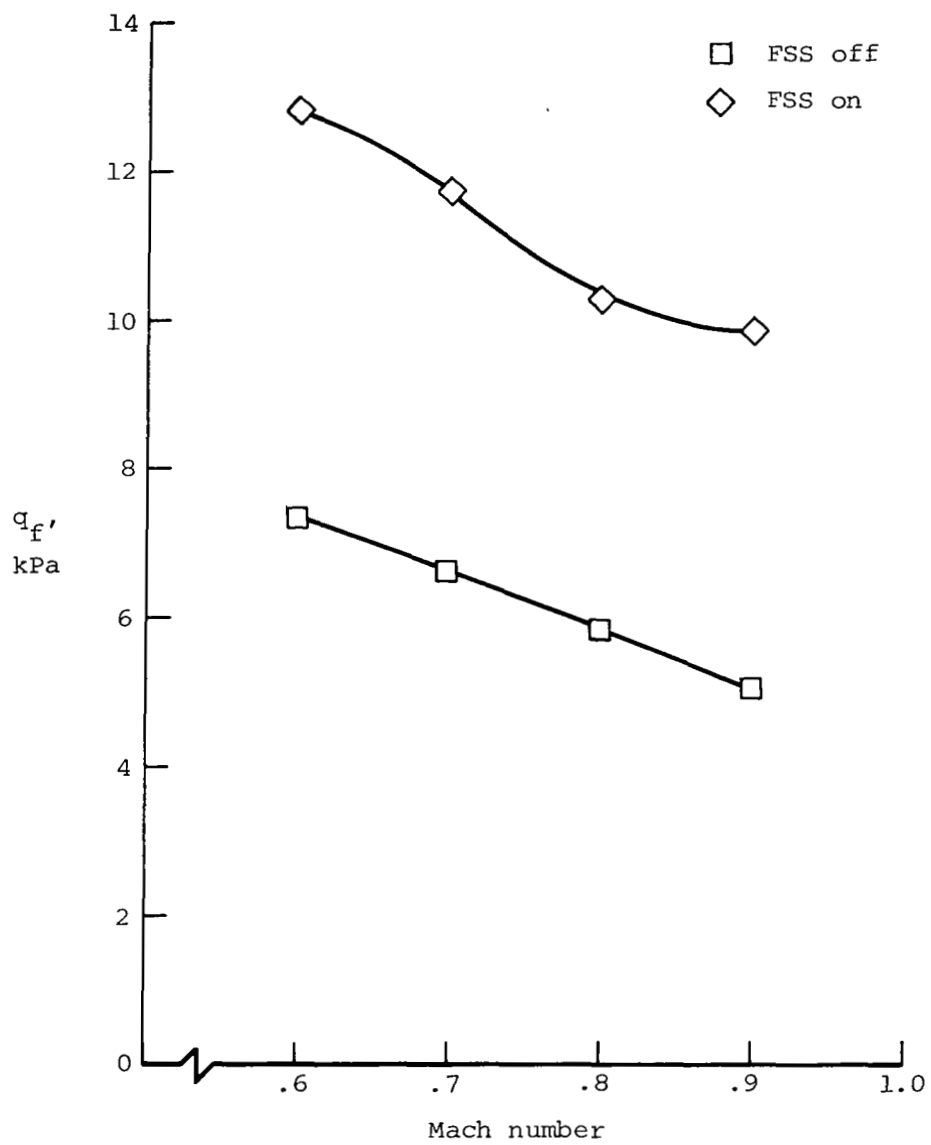(Arrows indicate increasing dynamic pressure.)

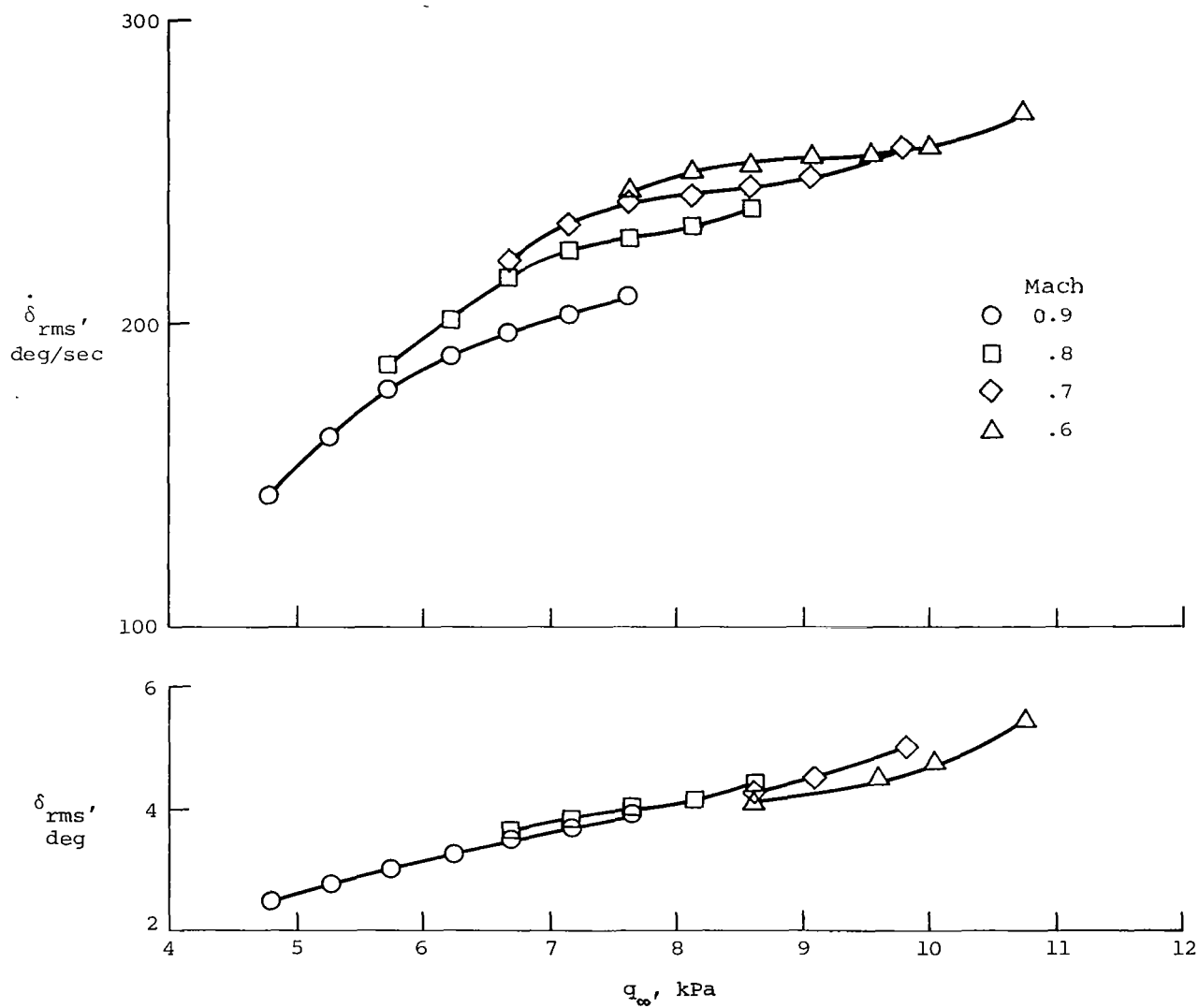Figure 12.- Flutter boundary; FSS off and FSS on.

Figure 13.- Variation with dynamic pressure of rms response to control activity.

1. Report No. NASA TP-1471	2. Government Accession No.	3. Recipient's Catalog No.
4. Title and Subtitle A METHOD FOR OBTAINING PRACTICAL FLUTTER-SUPPRESSION CONTROL LAWS USING RESULTS OF OPTIMAL CONTROL THEORY		5. Report Date August 1979
		6. Performing Organization Code
7. Author(s) Jerry R. Newsom		8. Performing Organization Report No. L-12728
9. Performing Organization Name and Address NASA Langley Research Center Hampton, VA 23665		10. Work Unit No. 505-02-33-05
		11. Contract or Grant No.
12. Sponsoring Agency Name and Address National Aeronautics and Space Administration Washington, DC 20546		13. Type of Report and Period Covered Technical Paper
		14. Sponsoring Agency Code

15. Supplementary Notes

16. Abstract

A method is presented for using the results of optimal control theory to synthesize a feedback filter. The feedback filter is used to force the output of the filtered frequency response to match that of a desired optimal frequency response over a finite frequency range. This matching is accomplished by employing a nonlinear programing algorithm to search for the coefficients of the feedback filter that minimize the error between the optimal frequency response and the filtered frequency response. The method is applied to the synthesis of an active flutter-suppression control law for an aeroelastic wind-tunnel model. It is shown that the resulting control law suppresses flutter over a wide range of subsonic Mach numbers. The study indicates that this is a promising method for synthesizing practical control laws using the results of optimal control theory.

17. Key Words (Suggested by Author(s)) Flutter suppression Aeroelasticity Optimal control theory	18. Distribution Statement Unclassified – Unlimited Subject Category 39

19. Security Classif. (of this report) Unclassified	20. Security Classif. (of this page) Unclassified	21. No. of Pages 31	22. Price* $4.50